Research Article | Vol. 25, No. 17 | 21 Aug 2017 | OPTICS EXPRESS 20381
Optics EXPRESS

Robust and efficient multi-frequency temporal phase unwrapping: optimal fringe frequency and pattern sequence selection

MINLIANG ZHANG,[1,2,3,4] QIAN CHEN,[1,2,5] TIANYANG TAO,[1,2,3] SHIJIE FENG,[1,2,3] YAN HU,[1,2,3] HUI LI,[1,2,3] AND CHAO ZUO[1,2,3,*]

[1] *School of Electronic and Optical Engineering, Nanjing University of Science and Technology, No. 200 Xiaolingwei Street, Jiangsu Province 210094, China*
[2] *Jiangsu Key Laboratory of Spectral Imaging and Intelligent Sense, Nanjing, Jiangsu Province 210094, China*
[3] *Smart Computational Imaging Laboratory (SCIlab), Nanjing University of Science and Technology, Nanjing, Jiangsu Province 210094, China*
[4] *z0712ml@163.com*
[5] *chenqian@njust.edu.cn*
[*] *surpasszuo@163.com*

Abstract: Temporal phase unwrapping (TPU) is an essential algorithm in fringe projection profilometry (FPP), especially when measuring complex objects with discontinuities and isolated surfaces. Among others, the multi-frequency TPU has been proven to be the most reliable algorithm in the presence of noise. For a practical FPP system, in order to achieve an accurate, efficient, and reliable measurement, one needs to make wise choices about three key experimental parameters: the highest fringe frequency, the phase-shifting steps, and the fringe pattern sequence. However, there was very little research on how to optimize these parameters quantitatively, especially considering all three aspects from a theoretical and analytical perspective simultaneously. In this work, we propose a new scheme to determine simultaneously the optimal fringe frequency, phase-shifting steps and pattern sequence under multi-frequency TPU, robustly achieving high accuracy measurement by a minimum number of fringe frames. Firstly, noise models regarding phase-shifting algorithms as well as 3-D coordinates are established under a projector defocusing condition, which leads to the optimal highest fringe frequency for a FPP system. Then, a new concept termed frequency-to-frame ratio (FFR) that evaluates the magnitude of the contribution of each frame for TPU is defined, on which an optimal phase-shifting combination scheme is proposed. Finally, a judgment criterion is established, which can be used to judge whether the ratio between adjacent fringe frequencies is conducive to stably and efficiently unwrapping the phase. The proposed method provides a simple and effective theoretical framework to improve the accuracy, efficiency, and robustness of a practical FPP system in actual measurement conditions. The correctness of the derived models as well as the validity of the proposed schemes have been verified through extensive simulations and experiments. Based on a normal monocular 3-D FPP hardware system, our method enables high-precision unambiguous 3-D shape measurement with the highest fringe frequency up to 180 by using only 7 fringe patterns, achieving a depth precision $\sim 38\mu$m across a field of view of $400 \times 300 \times 400$ mm.

OCIS codes: (110.5086) Phase unwrapping; (110.2650) Fringe analysis; (110.6880) Three-dimensional image acquisition.

References and links

1. L. Chen and C. Huang, "Miniaturized 3D surface profilometer using digital fringe projection," Meas. Sci. Technol. **16**(5), 1061 (2005).
2. Z. Zhang, "Review of single-shot 3D shape measurement by phase calculation-based fringe projection techniques," Opt. Lasers Eng. **50**(8), 1097–1106 (2012).
3. S. Gorthi and P. Rastogi, "Fringe projection techniques: whither we are," Opt. Lasers Eng. **48**, 133–140 (2010).
4. X. Su and Q. Zhang, "Dynamic 3-D shape measurement method: a review," Opt. Lasers Eng. **48**(2), 191–204 (2010).
5. X. Su and W. Chen, "Fourier transform profilometry: a review," Opt. Lasers Eng. **35**(5), 263–284 (2001).

#297395 https://doi.org/10.1364/OE.25.020381
Journal © 2017 Received 6 Jun 2017; revised 4 Aug 2017; accepted 4 Aug 2017; published 14 Aug 2017

Optics EXPRESS

6. Z. Zhang, C. Towers, and D. Towers, "Time efficient color fringe projection system for 3D shape and color using optimum 3-frequency selection," Opt. Express **14**(14), 6444–6455 (2006).
7. H. Li, G. Feng, P. Yang, Z. Wang, S. Zhou, and A. Asundi, "Online fringe projection profilometry based on scale-invariant feature transform," Opt. Eng. **55**(8), 084101 (2016).
8. K. Creath, "Step height measurement using two-wavelength phase-shifting interferometry," Appl. Opt. **26**(14), 2810–2816 (1987).
9. V. Gushov and Y. Solodkin, "Automatic processing of fringe patterns in integer interferometers," Opt. Lasers Eng. **14**(4), 311–324 (1991).
10. L. Kinell, and M. Sjödahl, "Robustness of reduced temporal phase unwrapping in the measurement of shape," Appl. Opt. **40**(14), 2297–2303 (2001).
11. X. Peng, Z. Yang, and H. Niu, "Multi-resolution reconstruction of 3-D image with modified temporal unwrapping algorithm," Opt. Commun. **224**(1), 35–44 (2003).
12. J. Tian, X. Peng, and X. Zhao, "A generalized temporal phase unwrapping algorithm for three-dimensional profilometry," Opt. Lasers Eng. **46**(4), 336-342 (2008).
13. C. Towers, D. Towers, and J. Jones, "Time efficient Chinese remainder theorem algorithm for full-field fringe phase analysis in multi-wavelength interferometry," Opt. Express **12**(6), 1136–1143 (2004).
14. S. Xing and H. Guo, "Temporal phase unwrapping for fringe projection profilometry aided by recursion of Chebyshev polynomials," Appl. Opt. **56**(6), 1591–1602 (2017).
15. L. Huang, J. Xue, B. Gao, C. McPherson, J. Beverage, and M. Idir, "Modal phase measuring deflectometry," Opt. Express **24**(21), 24649–24664 (2016).
16. C. Zuo, L. Huang, M. Zhang, Q. Chen, and A. Asundi, "Temporal phase unwrapping algorithms for fringe projection profilometry: A comparative review," Opt. Lasers Eng. **85**, 84–103 (2016).
17. T. Tao, Q. Chen, J. Da, S. Feng, Y. Hu, and C. Zuo, "Real-time 3-D shape measurement with composite phase-shifting fringes and multi-view system," Opt. Express **24**(18), 20253–20269 (2016).
18. J. Li, L. Hassebrook, and C. Guan, "Optimized two-frequency phase-measuring-profilometry light-sensor temporal-noise sensitivity," J. Opt. Soc. Am. A **20**(1), 106–115 (2003).
19. S. Zhang, "Phase unwrapping error reduction framework for a multiple-wavelength phase-shifting algorithm," Opt. Eng. **48**(10), 105601 (2009).
20. T. Tao, Q. Chen, S. Feng, Y. Hu, J. Da, and C. Zuo, "High-precision real-time 3D shape measurement using a bi-frequency scheme and multi-view system," Appl. Opt. **56**(13), 3646–3653 (2017).
21. H. Guo and B. Lü, "Phase-shifting algorithm by use of Hough transform," Opt. Express **20**(23), 26037–26049 (2012).
22. K. Qian, H. Miao, and X. Wu, "Real-time polarization phase shifting technique for dynamic deformation measurement," Opt. Lasers Eng. **31**(4), 289–295 (1999).
23. C. Zuo, Q. Chen, G. Gu, S. Feng, F. Feng, R. Li, and G. Shen, "High-speed three-dimensional shape measurement for dynamic scenes using bi-frequency tripolar pulse-width-modulation fringe projection," Opt. Lasers Eng. **51**(8), 953–960 (2013).
24. Y. Hu, Q. Chen, S. Feng, T. Tao, H. Li, and C. Zuo, "Real-time microscopic 3-D shape measurement based on optimized pulse-width-modulation binary fringe projection," Meas. Sci. Technol. **28**(7), 075010 (2017).
25. J. Huntley and H. Saldner, "Temporal phase-unwrapping algorithm for automated interferogram analysis," Appl. Opt. **32**(17), 3047-3052 (1993).
26. V. Srinivasan, H. Liu, and M. Halioua, "Automated phase-measuring profilometry of 3-D diffuse objects," Appl. Opt. **23**(18), 3105–3108 (1984).
27. X. Su, G. Von Bally, and D. Vukicevic, "Phase-stepping grating profilometry: utilization of intensity modulation analysis in complex objects evaluation," Opt. Commun. **98**(1-3), 141-150 (1993).
28. S. Zhang and S. Yau, "High-resolution, real-time 3D absolute coordinate measurement based on a phase-shifting method," Opt. Express **14**(7), 2644–2649 (2006).
29. P. Huang and S. Zhang, "Fast three-step phase-shifting algorithm," Appl. Opt. **45**(21), 5086–5091 (2006).
30. S. Feng, Y. Zhang, Q. Chen, C. Zuo, R. Li, and G. Shen, "General solution for high dynamic range three-dimensional shape measurement using the fringe projection technique," Opt. Lasers Eng. **59**, 56–71 (2014).
31. T. Petković, T. Pribanić, and M. Đonlić, "Temporal phase unwrapping using orthographic projection," Opt. Lasers Eng. **90**, 34–47 (2017).
32. X. Liu and J. Kofman, "Background and amplitude encoded fringe patterns for 3D surface-shape measurement," Opt. Lasers Eng. **94**, 63-69 (2017).
33. P. De Groot, "Derivation of algorithms for phase-shifting interferometry using the concept of a data-sampling window," Appl. Opt. **34**(22), 4723-4730 (1995).
34. Y. Surrel, "Design of algorithms for phase measurements by the use of phase stepping," Appl. Opt. **35**(1), 51–60 (1996).
35. R. Juarez-Salazar, F. Guerrero-Sanchez, and C. Robledo-Sanchez, "Theory and algorithms of an efficient fringe analysis technology for automatic measurement applications," Appl. Opt. **54**(17), 5364–5364 (2015).
36. J. A. Quiroga, J. A. Gómez-Pedrero, and Á. García-Botella, "Algorithm for fringe pattern normalization," Opt. Commun. **197**(1), 43–51 (2001).
37. C. Zuo, Q. Chen, G. Gu, S. Feng, and F. Feng, "High-speed three-dimensional profilometry for multiple objects with

Optics EXPRESS

complex shapes," Opt. Express **20**(17), 19493–19510 (2012).
38. S. Zhang and P. Huang, "Novel method for structured light system calibration," Opt. Eng. **45**(8), 083601 (2006).
39. K. Liu, Y. Wang, D. Lau, Q. Hao, and L. Hassebrook, "Dual-frequency pattern scheme for high-speed 3-D shape measurement," Opt. Express **18**(5), 5229–5244 (2010).
40. C. Zuo, Q. Chen, S. Feng, F. Feng, G. Gu, and X. Sui, "Optimized pulse width modulation pattern strategy for three-dimensional profilometry with projector defocusing," Appl. Opt. **51**(19), 4477–4490 (2012).
41. Y. Wang and S. Zhang, "Optimal pulse width modulation for sinusoidal fringe generation with projector defocusing," Opt. Lett. **35**(24), 4121–4123 (2010).
42. B. Pan, K. Qian, L. Huang, and A. Asundi, "Phase error analysis and compensation for nonsinusoidal waveforms in phase-shifting digital fringe projection profilometry," Opt. Lett. **34**(4), 416–418 (2009).

1. Introduction

Fringe projection profilometry (FPP) has been extensively developed for obtaining non-contact 3-D shape measurements in a variety of fields including mechanical engineering, industrial monitoring, computer vision, virtual reality, biomedicine and other industrial applications [1–7]. In FPP, temporal phase unwrapping (TPU) is an essential procedure to recover an unambiguous absolute phase even in the presence of large discontinuities or spatially isolated surfaces [8–17]. So far, there are typically three groups of TPU algorithms [16]: multi-frequency (hierarchical) approach [10–12], multi-wavelength (heterodyne) approach [8], and number-theoretical approach [9, 13]. We have detailedly discussed the noise-resistance ability of these three approaches in the comparative review [16], proving out that multi-frequency approach has the strongest resistance towards temporal noise.

For a practical FPP system, in order to achieve an accurate, efficient, and reliable measurement, one needs to make wise choices about three key experimental parameters: the highest fringe frequency, the phase-shifting steps, and the fringe frequency sequence. In this work, the fringe frequency represents the total number of periods in the fringe pattern, with the unit of periods per frame. The first parameter we talk about is the highest frequency. Generally speaking, higher fringes frequency leads to higher precision of 3-D reconstruction [16, 18], so increasing the fringe frequency is the most frequently used method to improve measurement results in FPP system [19, 20]. However, we find that because of the imperfection of the projection system, projector defocusing is unavoidable, which suppresses the modulation of fringe patterns especially when the fringe frequency is high. The reduction of the fringe modulation increases the phase noise, thereby reducing the 3-D measurement precision. According to our analysis, higher fringe frequency does not necessarily give better measurements. The second parameter we talk about is phase-shifting steps. Phase-shifting profilometry (PSP) is the most widely used methods to obtain phase [21, 22]. There are two main trends in the application of PSP: one is in real-time dynamic FPP system, which often chooses phase-shifting algorithm with less steps number, such as "2+3" (two low-frequency fringe patterns and three high-frequency fringe patterns) scheme, which is also termed of bi-frequency scheme [23]; another is in static high-precision FPP system, which often chooses phase-shifting algorithm with more steps number, such as "4+4+4+12" [24]. Are there any other differences between these different phase-shifting steps in addition to different degrees of suppression on noise? What is the difference between "2+3" and "3+2" (three low-frequency fringe patterns and two high-frequency fringe patterns) for 5 frames fringe patterns to measure phase? For a FPP system that pursues both precision and efficiency, which phase-shifting algorithm is the most cost-effective? These very interesting questions are rarely discussed in previous work. The last parameter we talk about is fringe frequency sequence. A commonly used fringe frequency sequence is {1, 2, 4, 8, ...} [19], which increases in the form of an exponential power of 2, and has a strong anti-noise capability, but it will undoubtedly result in huge time costs [25]. In order to improve the measurement efficiency, it seems that the fringe frequency sequence {1, 10, 100} with a larger exponential power of 10 should be used. This practice is very reasonable when the projector is focusing. However, the

Optics EXPRESS

actual projection system often has a certain degree of defocusing effect. In this case, even if the same phase-shifting steps are used, the noise of the wrapped phases corresponding to the fringes of the three frequencies are gradually increased. Therefore, noise effects in process of using the absolute phase of single-period fringes to unwrap the wrapped phase of 10-period fringes is not equivalent to that in process of using the absolute phase of 10-period fringes to unwrap the wrapped phase of 100-period fringes. In view of the above three issues, we believe that for an actual FPP system, to achieve high efficiency, high precision and robust 3-D measurement, the following three questions should be taken into account: (1) Is the fringe frequency really the higher the better? (2) Which phase-shifting combination is the most cost-effective in multi-frequency approaches? (3) Whether the exponentially incrementing fringe frequency sequence gives the best performance in terms of both robustness and efficiency?

For the first question, we establish noise models about phase-shifting algorithms as well as 3-D coordinates considering the effect of projector defocusing. According to these models, the attenuation effect of fringe modulation can be more obvious than the enhancement effect of fringe frequency when the fringe frequency is high. This indicates that the fringe frequency is not the higher the better, but there is a compromise in it. And we determine the optimal frequency f_{opt} by rigorous mathematical analysis and experimental verification. For the second question, we define a new concept termed frequency-to-frame ratio (FFR), which can be used to evaluate the magnitude of the contribution of each frame for TPU. According to the FFR, two-step phase-shifting (the algorithm used in bi-frequency scheme, we will make a detailed explanation later) is the most cost-effective. And a phase-shifting combination scheme which is beneficial to the FPP system to achieve the highest measurement efficiency is proposed. Minimum number of fringe frames are used to realize high precision measurement by the phase-shifting combination scheme. For the last question, we establish a judgment criterion, which can be used to judge whether the ratio between adjacent fringe frequencies is conducive to stably and efficiently unwrapping the phase. According to this criterion, the high frequency can be estimated based on the noise variance of low-frequency absolute phase, and a fringe frequency scheme is proposed based on the criterion. Combination of efficiency and robustness of FPP system can be achieved by the fringe frequency scheme.

This work provides a simple and effective theoretical framework to improve the accuracy, efficiency, and robustness of a practical FPP system in actual measurement conditions. For different FPP systems, the optimal fringe frequency and frequency sequence are different, but the method and procedure to select the optimal scheme complying with the same principle. For our system, the optimal fringe frequency is 180 periods/frame, the phase-shifting combination is 2-2-3, and the fringe frequency sequence is {1, 15, 180}. The correctness of the derived models as well as the validity of the proposed schemes have been verified through extensive simulations and experiments.

2. Principle

In this section, we detail our technique in four aspects. Firstly, PSP is introduced as a basis, and based on which we derive the noise models about PSP as well as 3-D coordinates. Then, we briefly introduce TPU, as well as the condition that should be satisfied in the TPU process. Further, we present the effect of projector defocusing, and incorporate it into the noise models. Finally, we determine the optimal frequency f_{opt} by the noise models, and propose a strategy to determine the optimal pattern sequence.

2.1. Phase-shifting profilometry

PSP is the most widely used methods to get phase at present [26–32]. And it provides high measurement resolution and precision since it can eliminates interferences from ambient light and surface reflectivity. In PSP, multiple phase-shifting sinusoidal fringe patterns are projected

Optics EXPRESS

sequentially by the projector onto an object surface and captured by the camera. The deformed fringes captured by the camera can be represented as:

$$I_n = A + B\cos(\varphi - 2\pi n/N) \tag{1}$$

where A is the average intensity relating to the pattern brightness and background illumination, B is the intensity modulation relating to the pattern contrast and surface reflectivity, N is the total number of phase-shifting steps, n is phase-shifting index and $n = 0, 1, \ldots, N-1$, and φ is the corresponding wrapped phase map which can be extracted by the following [33, 34]:

$$\varphi = \tan^{-1}\frac{\sum_{n=0}^{N-1} I_n \sin(2\pi n/N)}{\sum_{n=0}^{N-1} I_n \cos(2\pi n/N)}. \tag{2}$$

Since there are three unknowns A, B and φ in Eq. (2), at least three images should be used to calculate φ, namely $N \geq 3$. The intensity modulation B, is calculated to remove the unreliable points with weak reflectivity [23], which can be obtained by only a single frame in these meaningful works [35, 36]. However, in our work, we choose more commonly used method in PSP to calculate the intensity modulation B:

$$B = \frac{2}{N}\sqrt{[\sum_{n=0}^{N-1} I_n \sin(2\pi n/N)]^2 + [\sum_{n=0}^{N-1} I_n \cos(2\pi n/N)]^2} \tag{3}$$

Generally speaking, two or more different frequencies fringe patterns are utilized in TPU, and the average intensity A of different frequencies fringe patterns are almost same. Therefore, there are redundant information in fringe patterns with different frequencies. In order to utilize this information redundancy, bi-frequency scheme is proposed in [23], reducing the fringe patterns from N to 2. The average intensity A can be obtained by any set of sinusoidal patterns meeting condition of $N \geq 3$:

$$A = \frac{\sum_{n=0}^{N-1} I_n}{N} \tag{4}$$

The another two fringe patterns can be expressed as:

$$i_1 = A + B\sin(\varphi) \tag{5}$$

$$i_2 = A + B\cos(\varphi) \tag{6}$$

Then, the wrapped phase can be obtained from the following [23]:

$$\varphi = \tan^{-1}\frac{i_1 - A}{i_2 - A} \tag{7}$$

This algorithm is different from the standard N-step phase-shifting algorithm, for convenience of narration, we call it two-step phase-shifting algorithm. Using this method of two-step phase-shifting can reduce the number of fringe patterns, thereby improving the efficiency of measurement. But at least one set of fringe patterns meeting condition of $N \geq 3$ are needed to provide average intensity for this algorithm.

In fact, PSP not only can be used to get the phase, but also is a temporal filter, and the phase-shifting steps number reflects the size of the filter window. Much more phase-shifting steps have more obvious effect of noise suppression. The noise sources include ambient light, shadowing, projector illumination noise, camera or projector flicker, and quantization error in the frame grabber and the projector. In order to facilitate theoretical analysis, researchers assume a Gaussian distributed additive noise with a mean of zero and a variance of σ^2. When the sensor

Optics EXPRESS

noise is small compared to the true intensity signal, its effect can be considered as a small perturbation on the measured phase, which leads to the following approximation of the variance of phase error [16, 37]:

$$\sigma_{\Delta\varphi}^2 = \begin{cases} \frac{(N+1)\sigma^2}{NB^2}, & \text{2-step phase-shifting;} \\ \frac{2\sigma^2}{NB^2}, & \text{standard } N\text{-step phase-shifting.} \end{cases} \tag{8}$$

For the case of 2-step phase-shifting, $N(\geq 3)$ is the number of phase-shifting steps of the fringe patterns that provide the average intensity. According to Eq. (8), we can find that the signal-to-noise ratio of N-step phase-shifting is much better than that of 2-step phase-shifting. When we map the phase to the real world 3-D coordinates, the error variance of 3-D coordinates $\sigma_{\Delta P}^2$ can be further reduced by a factor of f^2 [16]:

$$\sigma_{\Delta P}^2 \propto \frac{\sigma_{\Delta\varphi}^2}{f^2} = \begin{cases} \frac{(N+1)\sigma^2}{Nf^2B^2}, & \text{2-step phase-shifting;} \\ \frac{2\sigma^2}{Nf^2B^2}, & \text{standard } N\text{-step phase-shifting.} \end{cases} \tag{9}$$

where f is the fringe frequency.

2.2. Temporal phase unwrapping

Since the arctangent function only ranges from $-\pi$ to π, phase unwrapping is necessary to eliminate the ambiguities of the phase in Eq. (2) and Eq. (7). The rudimentary phase unwrapping procedure is revealed as a process concerned with traversing through the wrapped phase vector sequentially in the x direction and adding or subtracting integer multiples of 2π [25]. This results in an unwrapped phase map which is given by Eq. (10):

$$\Phi = \varphi + 2\pi k \tag{10}$$

where Φ is the unwrapped phase, and k is the integer number called fringe orders. The key of phase unwrapping is to solve the fringe order k, which can be acquired from:

$$k = Round[\frac{f_h/f_l\Phi_l - \varphi_h}{2\pi}] \tag{11}$$

where $Round[\,]$ denotes to obtain the closest integer value, f_l and f_h are the low and high frequency respectively. Φ_l is the unwrapped phase of low-frequency fringes, and it severs as auxiliary phase to help unwrap the phase of high-frequency fringes, φ_h is the wrapped phase of high-frequency fringes. By this means the high-frequency phase φ_h can be unwrapped.

The key to phase unwrapping is to determine the fringe order of each pixel. In order to accurately unwrap the wrapped phase, it should be guaranteed that fringe order error $\Delta k = 0$, so there are [18]:

$$|\frac{f_h}{f_l}\Delta\Phi_l - \Delta\varphi_h| < \pi \tag{12}$$

Once the upper limit of $|\frac{f_h}{f_l}\Delta\Phi_l - \Delta\varphi_h|$ is less than or equal to π, i.e.:

$$\frac{f_h}{f_l}|\Delta\Phi_l|_{max} + |\Delta\varphi_h|_{max} \leq \pi \tag{13}$$

Then a sufficient condition about Eq. (12) is naturally gained. Most frequently, the 3-sigma rule of thumb is used in the empirical sciences, which expresses a conventional heuristic that "nearly all" values are taken to lie within three standard deviations of the mean, that is, to treat 99.73% probability as "near certainty". However, in FPP applications, we prefer to adopt a stricter limit at

Optics EXPRESS

4.5-sigma (99.9993% confidence) to get a more robust result [16]. Therefore, it can be considered that $|\Delta\Phi_l|_{max} = 4.5\sigma_{\Delta\Phi_l}$, $|\Delta\varphi_h|_{max} = 4.5\sigma_{\Delta\varphi_h}$. Thus Eq. (13) can be rewritten as:

$$\frac{f_h}{f_l}\sigma_{\Delta\Phi_l} + \sigma_{\Delta\varphi_h} \leq \frac{\pi}{4.5} \tag{14}$$

(14) is a criterion used to check whether the phase unwrapping results are reliable.

After the absolute phase of the highest frequency fringes is obtained through TPU, then the horizontal coordinate of corresponding points in projector can be calculated [20]:

$$x_p = \frac{p_w\Phi}{2\pi f} \tag{15}$$

where p_w is the horizontal resolution of projector, f is the frequency of the fringes. To determine the 3-D coordinates of each point of the object, system calibration should be performed [38]. Once the system calibration is done, the parameter matrix of the camera and the projector can be obtained, by which we can map the x_p to real world 3-D coordinates of the object through triangulation [39].

2.3. Projector defocusing effect

According to Eq. (9), the frequency of fringes is selected as higher as possible for improvement of measurement precision. However, we find that the frequency should not be increased arbitrarily not only due to the limitation of the resolution of projector but also more importantly the negative effect of projector defocusing which reduces the signal strength for excessively dense patterns. The defocusing effect can be considered as the convolution of the ideal gray distribution of the object with the point spread function of the projector system. The point spread function can usually be approximated as a Gaussian function [40, 41], and is actually a low-pass filter which has more attenuation on higher frequency signals. For sinusoidal fringes, its modulation is attenuated by the projector system:

$$B(f) = B_0H(f) = B_0exp(-2\pi^2\sigma_g^2f^2) \tag{16}$$

where f is fringe frequency, $B(f)$ is the modulation of the fringe patterns projected by projector, B_0 is the modulation of the fringe patterns sent to the projector system, which is generally pre-set, $H(f)$ is frequency response function of the system, σ_g is proportional to defocusing levels. In order to simulate the effect of the projector defocusing, we used MATLAB to generate sinusoidal fringe patterns with $B_0 = 127$, and $f = 1, 10, 20, ..., 250$, then applied a Gaussian filter with a size of 39×39 pixels and a standard deviation of 3 pixels for these sinusoidal fringes patterns to approximate the defocusing effect. $B(f)$ is calculated through Eq. (3), and the results are shown in Fig. 1(a). It can be seen from Fig. 1(a), the modulation of the fringe patterns declines following Gaussian function after the application of the Gaussian filter. When the fringe frequency is 50 periods/frame, the modulation is already reduced by 23.62% compared with the case of no blur. When the fringe frequency becomes 150 periods/frame, the modulation is reduced by as much as 91.34% compared with the case of no blur. Figures 1(b) and 1(c) are the fringe patterns of 100-period before and after the application of the Gaussian filter respectively. In order to avoid the misleading visual effects of excessive fringes, only a small portion of the whole fringe pattern is shown here. It is clear that Fig. 1(b) has a stronger contrast than Fig. 1(c). This means that projector defocusing makes the modulation of high-frequency fringe patterns a marked decline.

Equations (8) and (9) are noise model without considering the effect of projector defocusing which is negligible if the fringe frequency is very low. However, high-frequency fringes are often necessary for a high precision measurement, and the effect of projector defocusing becomes pronounced when the fringe frequency is high. So the noise model should be improved by

Optics EXPRESS

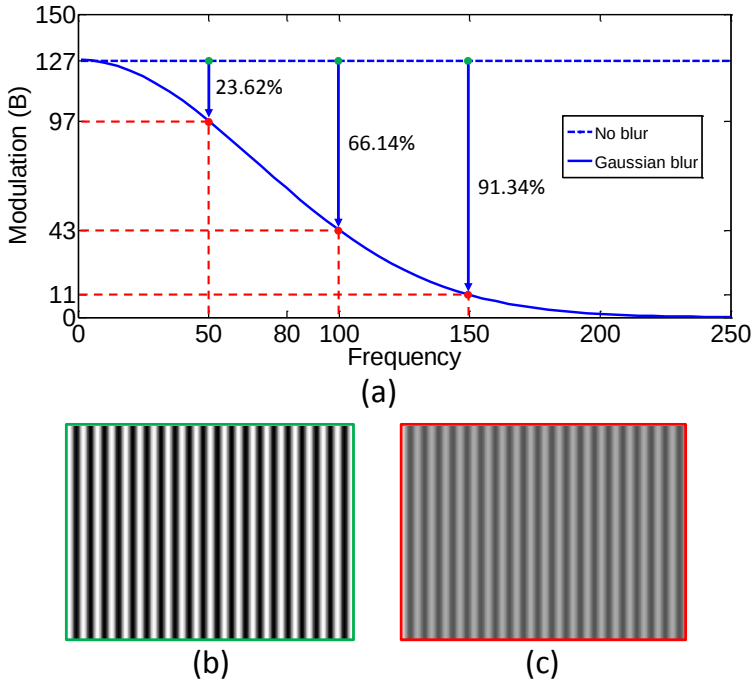

Fig. 1. (a) Influence of Gaussian blur on fringe modulation; (b) The fringe pattern of 100-period before the application of the Gaussian filter; (c) The fringe pattern of 100-period after the application of the Gaussian filter.

introducing the effect of projector defocusing. When the effect of projector defocusing is in consideration, Eq. (8) should be rewritten as:

$$\sigma_{\Delta\varphi}^2 = \begin{cases} \frac{(N+1)\sigma^2}{NB^2(f)}, & \text{2-step phase-shifting;} \\ \frac{2\sigma^2}{NB^2(f)}, & \text{standard } N\text{-step phase-shifting.} \end{cases} \tag{17}$$

Similarly, Eq. (9) should be rewritten as:

$$\sigma_{\Delta P}^2 \propto \frac{\sigma_{\Delta\varphi}^2}{f^2} = \begin{cases} \frac{(N+1)\sigma^2}{Nw^2}, & \text{2-step phase-shifting;} \\ \frac{2\sigma^2}{Nw^2}, & \text{standard } N\text{-step phase-shifting.} \end{cases} \tag{18}$$

where $w = fB(f)$. It can be seen from Eq. (18) that the noise variance of 3-D coordinates can be reduced by increasing the number of phase-shifting steps N and w when the light intensity noise is constant. Though increasing N can reduce the noise variance of 3-D coordinates, we do not recommend using this method because additional fringe patterns are required. The more cost-effective method is to increase w, which has much more precision enhancement than increasing N under the condition of the same consumption of fringes frames. According to Eq. (16), it can be known:

$$w = fB(f) = B_0 f exp(-2\pi^2\sigma_g^2 f^2) \tag{19}$$

If the projector is properly focused, namely $\sigma_g = 0$, then $w = B_0 f$. This means that after the projector defocusing introduced, the linearity relationship between w and f becomes nonlinear. To estimate the change of w with respect to f, we take derivative of f in Eq. (19):

$$w' = B_0 f exp(-2\pi^2\sigma_g^2 f^2)(1 - 4\pi^2\sigma_g^2 f^2) \tag{20}$$

Optics EXPRESS

Making $w' = 0$, it can be derived:

$$f = \frac{1}{2\pi\sigma_g} \tag{21}$$

According to the principle of differential, when $f = \frac{1}{2\pi\sigma_g}$, w will get the maximum value, which means that the optimal frequency f_{opt} for the fringe patterns is closely related to the degree of defocusing σ_g. Assuming that $\sigma_g = 0.001$ and $B_0 = 127$, the change of w with respect to f is shown in Fig. 2. As can be seen from Fig. 2, after the projector defocusing introduced, the linearity curve changes to a similar parabolic-like form, and there is always only one extreme point determining the optimal frequency. In the simulation case, the extreme point $f = 159$, which is the nearest integer from $\frac{1}{2\pi\sigma_g}$. When the frequency is 30 periods/frame, the value of w is 3743, which means that its 3-D measurement precision just reach 30.53% ($\frac{3743}{12260} \approx 30.53\%$) of the highest precision.

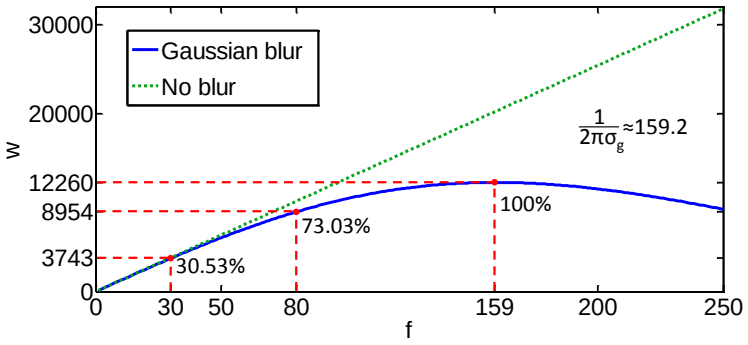

Fig. 2. The curve of the change of w ($= fB$) with respect to frequency f.

2.4. Pattern sequence selection strategy

As mentioned before, Eq. (14) is a criterion used to check whether the phase unwrapping results are reliable. In fact, on the other hand, for a specific set of fringe patterns, Eq. (14) can be used to estimate the range of high-frequency f_h in which the wrapped phase φ_h can be unwrapped correctly provided that the multiples relationship between $\sigma_{\Delta\varphi_h}$ and $\sigma_{\Delta\Phi_l}$ can be known in advance. As can be seen from Eq. (17), when 2-step phase-shifting is used to generate high-frequency fringe patterns, and N-step phase-shifting is used to generate low-frequency fringe patterns, the ratio of $\sigma_{\Delta\varphi_h}$ to $\sigma_{\Delta\Phi_l}$ will be maximized:

$$\frac{\sigma_{\Delta\varphi_h}}{\sigma_{\Delta\Phi_l}} \le \frac{\sqrt{\frac{(N+1)\sigma^2}{NB^2(f_h)}}}{\sqrt{\frac{2\sigma^2}{NB^2(f_l)}}} = \sqrt{\frac{N+1}{2}}\frac{B(f_l)}{B(f_h)} \tag{22}$$

where $B(f_l)$ represents the modulation of the low-frequency auxiliary fringe patterns and $B(f_h)$ represents the modulation of the high-frequency fringe patterns. From Eq. (22) we can see that there is a quantitative relationship between the noise of high-frequency fringe phase and the noise of low-frequency fringe phase. Thus, Eq. (14) can be rewritten as:

$$\frac{f_h}{f_l} \le \frac{\pi}{4.5\sigma_{\Delta\Phi_l}} - \sqrt{\frac{N+1}{2}}\frac{B(f_l)}{B(f_h)} \tag{23}$$

In the pattern sequence selection strategy we proposed, phase-shifting steps number N ranges from 2 to 4 (see the later section in this chapter for details) as listed in Table 2. So $N = 4$ should

Optics EXPRESS

be selected to substitute into Eq. (23) to make sure that the left value of the inequality is less than the minimum of the right value. The value of $\frac{B(f_l)}{B(f_h)}$ is equal to 1 if projector is properly focused, and it becomes greater than 1 when projector is defocused. Based on the results of experiment in section 3.1, we can find that $\frac{B(f_l)}{B(f_h)} \leq 4$ under nine different kinds of measurement conditions if $\frac{f_h}{f_l} \leq 200$. Besides, to improve the stability of phase unwrapping results, we assume that the phase noise variance in actual measurement is twice the detected phase noise variance, then Eq. (23) can be rewritten as:

$$\frac{f_h}{f_l} \leq \frac{2\pi}{9\sqrt{2}\sigma_{\Delta\Phi_l}} - 2\sqrt{10} \tag{24}$$

From Eq. (24), the range of $\frac{f_h}{f_l}$ can be calculated based on a premise that the noise standard deviation of auxiliary fringes $\sigma_{\Delta\Phi_l}$ can be known beforehand.

The purpose of selecting a pattern sequence is to stably achieve a high precision measurement with minimal fringe patterns. In order to better analyze the problem, we propose the concept of frequency-to-frame ratio (FFR). The fringe parameter pair (f, N) is used to represent a group of fringe patterns with frequency f and phase-shifting steps number N, and use $f_N^{f_l}(N = 2, 3, 4, \ldots)$ to represent the highest frequency fringe patterns whose wrapped phase can be correctly unwrapped by the auxiliary phase corresponding to fringe patterns (f_l, N). According to this definition, when the unambiguous absolute phase corresponding to the fringe patterns (f_l, N) is used as auxiliary phase, it can correctly unwrap the wrapped phase corresponding to the fringe patterns $(f_N^{f_l}, 3)$ but fails to unwrap the wrapped phase corresponding to the fringe patterns $(f_N^{f_l} + 1, 3)$, then the ratio $\frac{f_N^{f_l}}{f_l N}$ is the so-called FFR. Obviously, the value of FFR reflects the magnitude of the contribution of each frame for TPU and is determined by fringe parameter pair (f_l, N). Selecting the number of phase-shifting steps with high FFR can improve the efficiency of TPU. Assuming that the unambiguous absolute phase corresponding to the fringe patterns $(f_l, 3)$ is used as auxiliary phase, the wrapped phase corresponding to the fringe patterns $(f_h \leq f_3^{f_l}, 3)$ can be unwrapped correctly whereas the wrapped phase corresponding to the fringe patterns $(f_h > f_3^{f_l}, 3)$ can not be unwrapped correctly, then according to Eqs. (14) and (17), we can derive:

$$\frac{f_3^{f_l}}{f_l}\sqrt{\frac{2\sigma^2}{3B^2(f_l)}} = \frac{\pi}{4.5} - \sqrt{\frac{2\sigma^2}{3B^2(f_3^{f_l})}} \tag{25}$$

Similarly, assuming that the unambiguous absolute phase corresponding to the fringe patterns (f_l, N) is used as auxiliary phase, the wrapped phase corresponding to the fringe patterns $(f_h \leq f_N^{f_l}, 3)$ can be unwrapped correctly whereas the wrapped phase corresponding to the fringe patterns $(f_h > f_N^{f_l}, 3)$ can not be unwrapped correctly, then according to Eqs. (14) and (17), we can derive the following formula (if $N \leq 10$, it can be obtained that $B(f_N^{f_l}) \approx B(f_3^{f_l})$):

$$\frac{f_N^{f_l}}{f_l}\sqrt{\frac{2\sigma^2}{NB^2(f_l)}} = \frac{\pi}{4.5} - \sqrt{\frac{2\sigma^2}{3B^2(f_N^{f_l})}} \approx \frac{\pi}{4.5} - \sqrt{\frac{2\sigma^2}{3B^2(f_3^{f_l})}} = \frac{f_3^{f_l}}{f_l}\sqrt{\frac{2\sigma^2}{3B^2(f_l)}} \tag{26}$$

It is available from Eq. (26) that:

$$f_N^{f_l} \approx \sqrt{\frac{N}{3}} f_3^{f_l} \tag{27}$$

Thus we can derive the FFR corresponding to the fringe patterns (f_l, N):

$$FFR_N^{f_l} = \frac{f_N^{f_l}}{N f_l} \approx \frac{f_3^{f_l}}{\sqrt{3N} f_l} \approx \sqrt{\frac{3}{N}} FFR_3^{f_l} \qquad (N \geq 3) \tag{28}$$

Optics EXPRESS

Assuming that the unambiguous absolute phase corresponding to the fringe patterns $(f_l, 2)$ is used as auxiliary phase, following the above analysis we can derive that (in the derivation process we assume that $B(f_2^{fi}) \approx B(f_3^{fi})$):

$$f_2^{fi} \approx \frac{f_3^{fi}}{\sqrt{2}} \tag{29}$$

$$FFR_2^{fi} = \frac{f_2^{fi}}{2f_l} \approx \frac{f_3^{fi}}{f_l\sqrt{8}} \approx \frac{3}{2\sqrt{2}} FFR_3^{fi} \tag{30}$$

In order to verify our conclusion of FFR, we used MATLAB to generate sinusoidal fringes patterns with $(1, N)(N = 2, 3, 4, ..., 10)$, then applied a Gaussian filter with a size of 39×39 pixels and a standard deviation of 1.2 pixels for these sinusoidal fringes patterns to approximate the defocusing effect, finally added Gaussian noise with a mean of zero and variance of 0.0006 to these patterns. The absolute phase corresponding to fringe patterns $(1, N)$ is used as auxiliary phase to unwrap the wrapped phase corresponding to fringe patterns $(f, 3)$ (f=2, 3, 4, ..., 50), and the frequency f_N^{fi} is found by checking the unwrapped phase. The results are shown in Table 1, N=2 represents 2-step phase-shifting in bi-frequency scheme [23]. As can be seen from Table

Table 1. FFR of different number of phase-shifting steps.

Phase-shifting steps number(N)	2	3	4	5	6	7	8	9	10
Threshold frequency(f_N^1)	15	21	24	27	29	31	33	36	38
$FFR_N^1 (= \frac{f_N^1}{N})$	7.5	7	6	5.4	4.8	4.4	4.1	4	3.8

1, 2-step phase-shifting has the largest FFR, meaning that it has the highest cost-effective, so we should give priority to 2-step phase-shifting to improve measurement efficiency. But it should be noted that at least one set of fringe patterns whose phase-shifting steps number is not less than 3 are needed to provide average intensity.

Through the previous discussion, we summarize five basic requirements for determining the optimal fringe pattern sequence: (1) the highest frequency of the fringe patterns must be equal or close to f_{opt} to achieve high precision measurements; (2) the ratio between adjacent frequencies should not be greater than $\frac{f_N^{fi}}{f_l}$; (3) at least one set of fringe patterns meeting condition of $N \geq 3$ are needed to provide average intensity; (4) giving priority to 2-step phase-shifting, so four-step phase-shifting should be replaced by 2-2, and five-step phase-shifting should be replaced by 2-3 or 3-2; (5) giving priority to generating the highest frequency fringe patterns with larger number of phase-shifting steps, because increasing the number of phase-shifting steps can suppress phase random noise. Once these five requirements are met, the highest precision of the fringe projection measurement system can be achieved with minimal fringe patterns. Some of the optimal fringe pattern sequence are list in Table 2.

Explanations about the Table 2 (1) (×) represents that the combination is not being considered. Because the combination of 3-2 has been ruled out for $f_3^1 \leq f_{opt}$, so the combination of 2-4 and 3-3 should be ruled out too. (2) Bold numbers represent the phase-sifting steps number of auxiliary fringes, which determines the value of the highest frequency whose wrapped phase can be unwrapped correctly by the auxiliary fringes. (3) The order of the phase-shifting combination represents its priority, the corresponding frequency sequence is used to judge whether the phase-shifting combination can be used. (4) The order of the phase-shifting combination is arranged according to the ability of unwrapping wrapped phase.

Optics EXPRESS

Table 2. Fringe pattern sequence selection strategy.

Total frames	Phase-shifting combination	Frequency sequence
5	**2** – 3	$\{1, f_{opt}(\leq f_2^1)\}$
	3 – 2	$\{1, f_{opt}(\leq f_3^1)\}$
6	**2** – 4 (×)	$\{1, f_{opt}(\leq f_2^1)\}$ (×)
	3 – 3 (×)	$\{1, f_{opt}(\leq f_3^1)\}$ (×)
	4 – 2	$\{1, f_{opt}(\leq f_4^1)\}$
7	**2** – **2** – 3	$\{1, f_l(\leq f_2^1), f_{opt}(\leq f_2^{f_2^1})\}$
	3 – **2** – 2	$\{1, f_l(\leq f_3^1), f_{opt}(\leq f_2^{f_3^1})\}$
	2 – **3** – 2	$\{1, f_l(\leq f_2^1), f_{opt}(\leq f_3^{f_2^1})\}$
8	**2** – **2** – 4 (×)	$\{1, f_l(\leq f_2^1), f_{opt}(\leq f_2^{f_2^1})\}$ (×)
	2 – **3** – 3 (×)	$\{1, f_l(\leq f_2^1), f_{opt}(\leq f_3^{f_2^1})\}$ (×)
	4 – **2** – 2	$\{1, f_l(\leq f_4^1), f_{opt}(\leq f_2^{f_4^1})\}$
	2 – **4** – 2	$\{1, f_l(\leq f_2^1), f_{opt}(\leq f_4^{f_2^1})\}$
	3 – **3** – 2	$\{1, f_l(\leq f_3^1), f_{opt}(\leq f_3^{f_3^1})\}$
...	...	...

3. Experiment

The experiments are based on a 3D shape measurement system comprising a DMD projector (M115HD, Dell) and a CMOS camera (daA1280-54um, Basler) with a computar M1214-MP2 lens F/1.4 with focal length of 12 mm. The resolution of the camera is 1280 × 960, with a maximum frame rate of 54 frames per second. The projector has a resolution of 1280 × 720 with a lens of F/2.0 focal length of 14.95 mm. In order to reduce the influence of the non-linear response of the projector on the phase accuracy [42], gamma correction of the projector was performed by pre-distorting the ideal sinusoidal patterns based on a calibrated gamma curves stored in a LUT [37]. In the following experiments, objects are scanned with a camera exposure time of 33.33 ms.

3.1. Determining the value of f_{opt}

From Eq. (21), we can see that f_{opt} is greatly influenced by the degree of projector defocusing, so it is necessary to detect the degree of projector defocusing in the current state. However, in the actual measurement, besides the main impact by projector defocusing, the fringe modulation is also affected by camera exposure, the position of the measured object as well as projector pixel discretization and so on. These factors should also be considered to improve the previous model of modulation but they can not be analyzed theoretically. So in these experiments, we directly test the modulation of fringe patterns of different frequency projected by the projector. For the projector with horizontal resolution of 1280, the fringe frequency can be as high as 256 periods/frame (at least 5 pixels per fringe along the horizontal axis should be guaranteed to avoid spatial aliasing of the peaks and troughs of the sinusoidal intensity profile), instead of detecting and calculating so many frequencies one by one, we detect and calculate the fringe modulation $B(f)$ of fringe patterns with frequency 1, 5, 10, 20, 30, 40, 60, 100, 140, 180, 220 and 250 periods/frame reflected by standard ceramic plate. In order to highlight the change of fringe modulation with respect to fringe frequency, we normalized the fringe modulation by $\bar{B}(f) = \frac{B(f)}{B(1)}$. Here, $B(1)$ refers to the modulation of single-period fringes patterns and $\bar{B}(f)$

Optics EXPRESS

is the normalized modulation. $B(1)$ is constant under a specific measurement environment, so it will not change the value of f_{opt} and still can highlight the change of $(fB(f))^2$ with respect to fringe frequency f. To determine the impact of camera exposure and the position of the measured object, we separately detect the normalized modulation $\bar{B}(f)$ of these nine cases of which include weak exposure (A=42.8, $B(1)$=32.82, $B(1)$ refers to the modulation of single-period fringes patterns), medium exposure (A=79.31, $B(1)$=60.17) and strong exposure (A=128.55, $B(1)$=97.14), as well as close distance (400mm, referring to the distance between measured surface and projector), medium distance (550mm) and long distance (700mm), and three different angles ($0°, 30°and\ 60°$) between the measured surface and projector optical axis. The experimental results are shown in Fig. 3, and we can easily find that the measured results of different measurement conditions have large differences. In the actual measurement case, the measured surface of the object often have problems of different exposure, different distance and different angles. In order to improve the robustness of the system, we decide to find a frequency reference range. In this range, the product of the square of frequency f_{opt} and square of normalized modulation $\bar{B}(f_{opt})$ is not less than 90% of its own maximum value under above nine kinds of measurement conditions, i.e.: $0.9[f\ \bar{B}(f)]^2_{max} \leq [f_{opt}\ \bar{B}(f_{opt})]^2 \leq [f\ \bar{B}(f)]^2_{max}$. Once obtaining the frequency reference ranges that meet the requirement under these nine kinds of measurement conditions, the common range of these ranges will serve as the final reference range. In our experiments, the nine frequency ranges are [158, 256], [140, 230], [117, 191], [119, 193], [146, 237], [128, 204], [146, 237], [149, 237] and [166, 255], and the common range of these nine ranges is [166, 191]. Finally, we select the median value 180 of the common range as the value of f_{opt}. Of course, selecting other values in the common range is also acceptable.

3.2. Determining the optimal fringe pattern sequence

In section 3.1, we have determined the value of f_{opt}, which means the optimal precision can be obtained through 180-period fringes. Then comes the next step, confirming the efficient and robust measurement scheme, to realize the optimal measurement precision. The efficiency and stability of the measurement mainly depends on phase-shifting steps number and fringe frequency sequence. In section 2.4, we have determined all possible optimal phase-shifting combinations by quantitative analysis, and these possible optimal phase-shifting combinations are listed in Table 2. What we need to do is to inspect which one can satisfy requirements of the fringe frequency sequence. For example, when we intend to inspect phase-shifting combination 2-3, we should compare 180 with f_2^1, if $180 \leq f_2^1$, then phase-shifting combination 2-3 can satisfy requirements of the fringe frequency sequence $\{1, 180\}$. Obviously, f_2^1 is a criterion of judgment whether the combination 2-3 can be chosen, however, we can not obtain the value of it beforehand in the experiment. The value of f_N^{fi} is unknown in the experiment is an obstacle to our next step. Fortunately, Eq. (24) provides us with a method to overcome it. Based on Eq. (24), once the noise variance of the auxiliary phase is detected, it is possible to estimate the f_N^{fi} in the current state. We experimentally detect that the unambiguous absolute phase noise variance corresponding to the fringe patterns (1, 3) is approximately equal to 0.00028. Substituting $\sigma_{\Delta\Phi_l} = \sqrt{0.00028}$ and $f_l = 1$ into Eq. (24), we can derive $f_h \leq 24$, so f_3^1 is equal to 24. Substituting $f_3^1 = 24$ and $f_N^1 = f_{opt} = 180$ into Eq. (27), we can derive $N \approx 169$, which means that at least 169 fringe patterns are required to unwrap the wrapped phase corresponding to the fringe patterns (180, 3) using the single-period unambiguous absolute phase as auxiliary phase. Obviously, using bi-frequency fringe pattern sequence is not the optimal scheme, therefore, we do not consider the case where the total number of frames are 5 or 6 in Table 2. According to the order of the phase-shifting sequences listed in Table 2, we firstly consider the case where the total number of frames are 7, and give priority to 2-2-3 combination. We experimentally detect that the unambiguous absolute phase noise variance corresponding to the fringe patterns (1, 2)

Optics EXPRESS

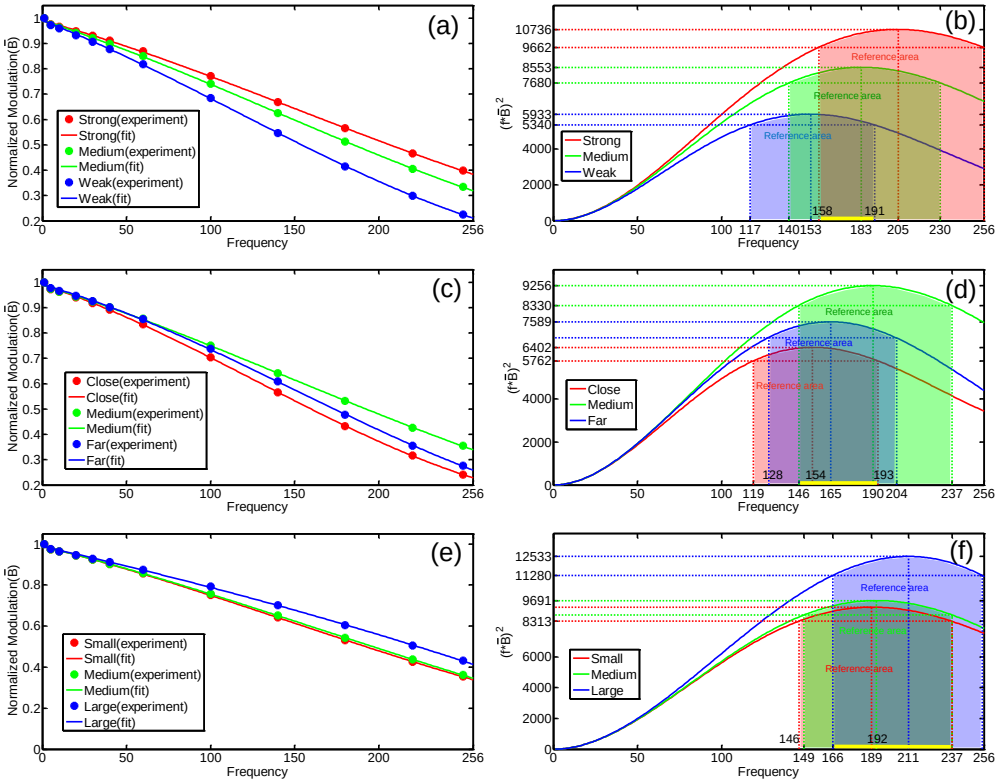

Fig. 3. (a),(c),(e) The normalized fringe modulation measured under different exposure, different distance, and different angles; (b),(d),(f) The product of the square of frequency and square of normalized modulation under different exposure, different distance ,and different angles. The background color region represents the reference ranges under different conditions, and the yellow line represents the common range of three reference range in the graph.

is approximately equal to 0.00053. Substituting $\sigma_{\Delta\Phi_l} = \sqrt{0.00053}$ and $f_l = 1$ into Eq. (24), we can derive $f_h \leq 16$, so f_2^1 is equal to 16. Then we experimentally detect that the unambiguous absolute phase noise variance corresponding to the fringe patterns (16, 2) is approximately equal to 0.0007. Substituting $\sigma_{\Delta\Phi_l} = \sqrt{0.0007}$ and $f_l = 16$ into Eq. (24), we can derive $f_h \leq 16 \times 13$, so $f_2^{16} = 208(16 \times 13)$. At last we choose frequency combination $\{1, 15, 180\}$ as the optimal frequency sequence.

Let us summarize the whole process of determining the optimal fringe pattern sequence. Firstly, test the modulation of different frequency fringe patterns and find the optimal frequency f_{opt} minimizing the 3-D coordinates noise. Then, starting from the case of 5 frames, inspect these phase-shifting combinations sequentially, once a phase-shifting combination meets the requirements, end the process, otherwise, inspect the next case of more frames. The whole process of determining the optimal fringe pattern sequence is shown in Fig. 4(a), and inspection process of phase-shifting combination 2-2-3 is shown as an example in Fig. 4(b). N_s represents the total number of fringe patterns.

Optics EXPRESS

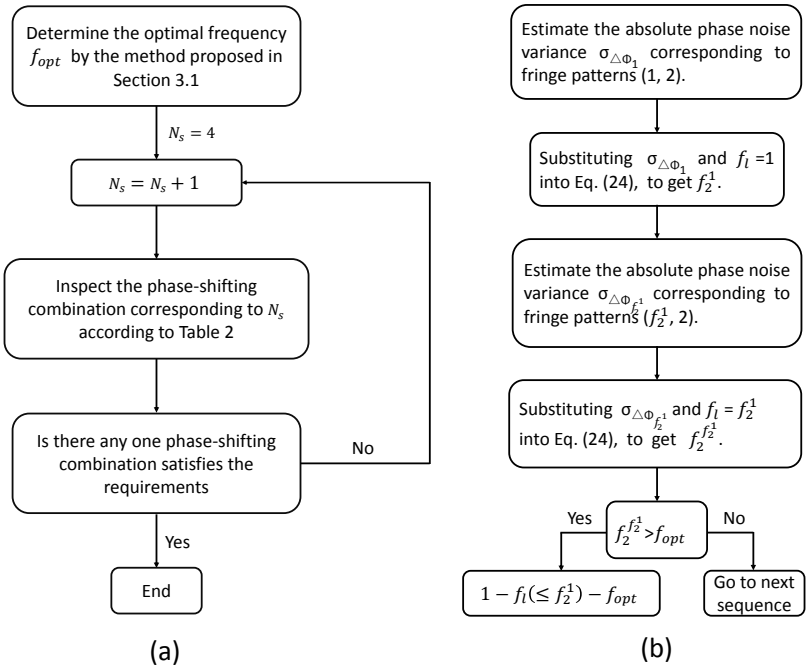

Fig. 4. (a) The whole process of determining the optimal fringe pattern sequence; (b) Inspection process of phase-shifting combination 2-2-3.

3.3. Experimental results

3.3.1. Comparison of anti-noise capability

To validate the robust anti-noise capability of the frequency sequence $\{1, 15, 180\}$, we reduced the exposure of the camera to increase intensity noise, and then measured a standard ceramic plate using fringe patterns with $\{1, 8, 180\}$, $\{1, 15, 180\}$ and $\{1, 25, 180\}$ respectively. Phase-shifting combination all are 2-2-3. The experimental results are shown in Fig. 5. It can be seen from Fig. 5, when increasing light intensity noise, the frequency sequence $\{1, 15, 180\}$ is still able to stably unwrap the phase, while the other two sequences have different number abnormal points. For frequency sequence $\{1, 8, 180\}$, the wrapped phase of 8-period fringes is correctly unwrapped with the help of the single-period auxiliary phase, but the absolute phase of 8-period fringes fails to unwrap the wrapped phase of 180-period fringes in some pixels. For frequency sequence $\{1, 25, 180\}$, the single-period phase fails to unwrap the wrapped phase of 25-period fringes in some pixels. The excessive ratio of adjacent frequencies which does not meet Eq. (24) is the failure reason of the two cases.

3.3.2. Comparison of measurement precision

According to Eq. (18), the noise of 3-D coordinates is in proportion to the normalized phase. In order to prove that the fringe patterns with frequency 180 periods/frame has the highest precision of normalized phase, we measured a standard ceramic plate using fringe patterns with $\{1, 15, 90\}$, $\{1, 15, 180\}$ and $\{1, 15, 256\}$ respectively, and phase-shifting combinations all are 2-2-3. After the phase data is obtained, we fitted it using a planar model to acquire quasi-standard phase data, and the differences between the measured surface and the fitted surface represent the phase errors. The experimental results are shown in Fig. 6, where the red and yellow planes represent $\pm 3\sigma_{\frac{\Delta\varphi}{f}}$, respectively, and we can easily find that the frequency combination $\{1, 15, 180\}$ has the smallest

Optics EXPRESS

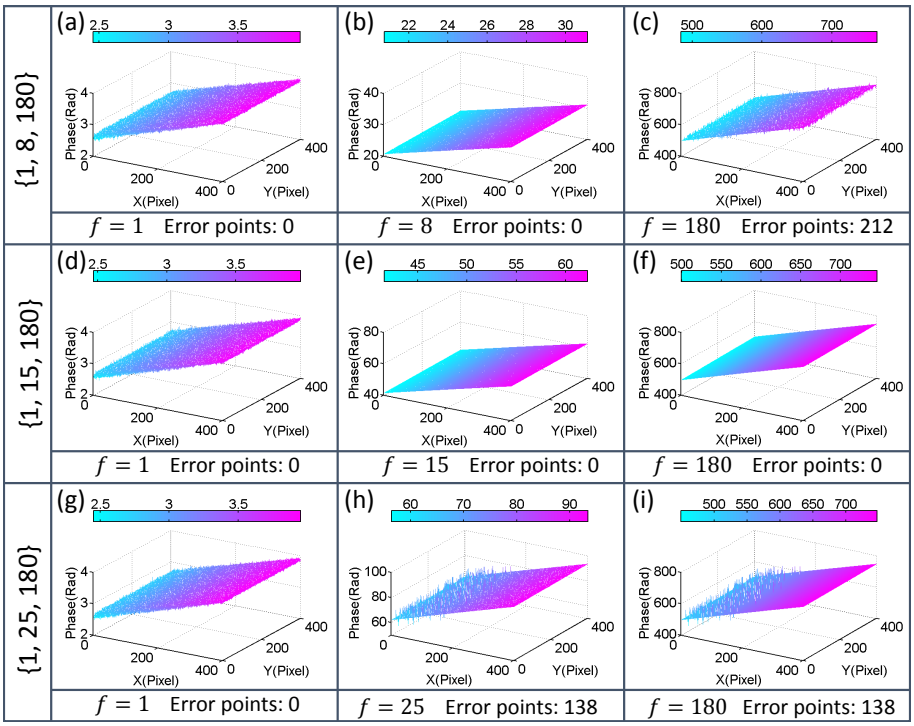

Fig. 5. Standard ceramic plate phase diagram. (a)~(c) {1, 8, 180}; (d)~(f) {1, 15, 180}; (g)~(i) {1, 25, 180}.

phase error.

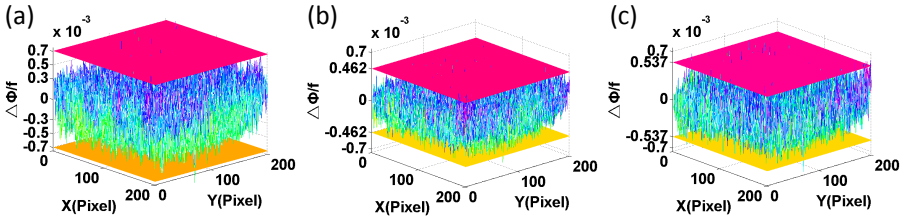

Fig. 6. Comparison of phase noise. (a) {1, 15, 90}; (b) {1, 15, 180}; (c) {1, 15, 256}.

To compare 3-D measurement precision of the three frequency sequences, we measured the standard sphere with radius R = 25.4 mm. After the sphere surface data is obtained, we fitted it using a spherical model to acquire quasi-standard sphere center. Standard sphere radius, the distance from the point on the sphere to the quasi-standard sphere center, are calculated according to the distance formula of the 3-D space. And the differences between the measured radius and the standard radius 25.4 mm represent the measurement errors. The measurement results are shown in Fig. 7. In Fig. 7(a), the three graphs in the first row show the calculation results of the standard sphere surface, the three graphs in the second row show the measurement results of radius of standard sphere and the three graphs in the third row show radius error. Figure 7(b) shows the probability distribution of the radius error.

Optics EXPRESS

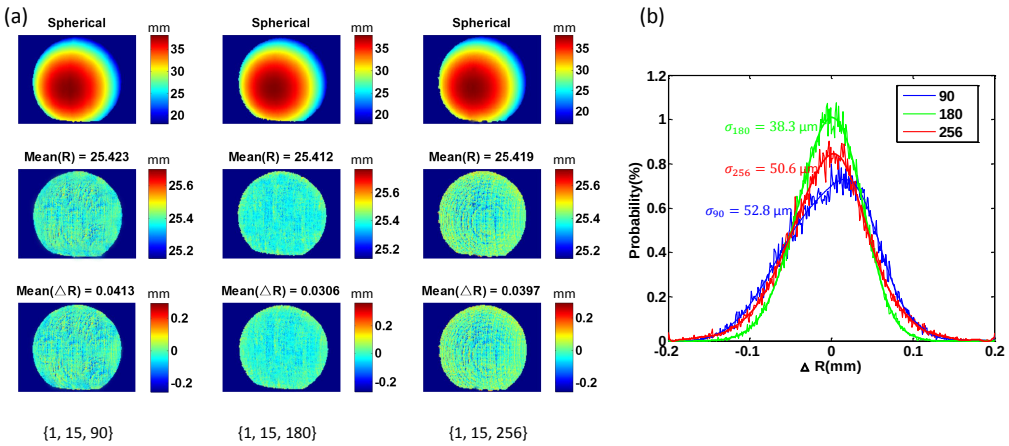

Fig. 7. Measurement results of standard sphere. (a) The reconstructed spherical surface, spherical radius and spherical radius error; (b) Probability distribution of radius error.

3.3.3. Comparison of 3-D topography of complex objects

In section 3.3.2, we chose the frequency sequences $\{1, 15, 90\}$, $\{1, 15, 180\}$ and $\{1, 15, 256\}$ to make a quantitative comparison. In this section, we will do a qualitative comparison among them. The model of David is measured in the experiments. As can be seen from the experimental results in Fig. 8, measurement result corresponding to frequency sequence $\{1, 15, 180\}$ is the best for the reason that its reconstructed surface is more smooth and no loss of details than other two. It is should also be noted that some holes appear in the surface measurement results in the shadow area, and obviously the higher the fringe frequency is, the more the number of holes appear. This arise from the fact that the fringe modulation decreases with the increase of fringe frequency due to projector defocusing. When the modulation decreases to small enough, the corresponding region will be filtered as background, thus holes are formed.

3.3.4. Measurement of human face

In order to further prove the feasibility and validity of our proposed method, human face with normal complexion was measured using the fringe patterns with frequency sequence $\{1, 15, 180\}$ and phase-shifting combination 2-2-3. The results are shown in Fig. 9. Due to the influence of human complexion, the measurement precision decreases a lot compared with those white objects. Despite this factor, the measurement precision is still very considerable because using the optimal fringe frequency. As can be seen in Fig. 9(b), some local features on the face such as naevi are still well preserved.

4. Conclusion

In this paper, we proposed a new scheme to determine the optimal fringe frequency and pattern sequence to realize high precision, high efficiency and robust measurement. Firstly, we established noise models about phase-shifting algorithms as well as 3-D coordinates under projector defocusing condition. According to the models, the projector defocusing has a more severe attenuation on the modulation of higher frequency fringes. So the precision of 3-D reconstruction reaches the maximum only when the product of fringe frequency and modulation reaches its maximum. We detected the modulation of twelve frequencies fringes under different representative measurement conditions, acquiring the optimal fringe frequency f_{opt} = 180 periods/frame that makes the product of the frequency and modulation reach more than 0.9 times

Optics EXPRESS

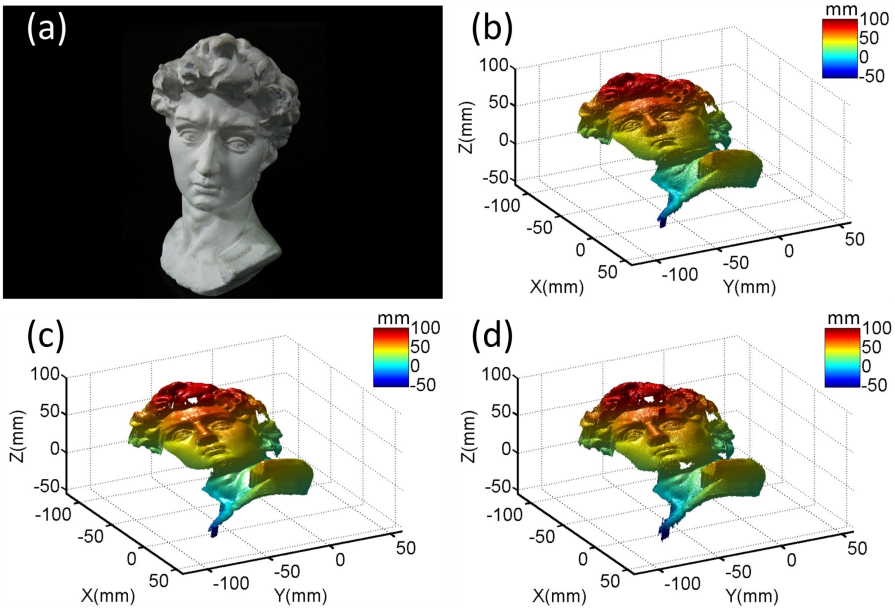

Fig. 8. David surface measurement. (a) The physical map of David; (b) The 3-D map of David surface when the frequency sequence is {1, 15, 90}; (c) The 3-D map of David surface when the frequency sequence is {1, 15, 180}; (d) The 3-D map of David surface when the frequency sequence is {1, 15, 256}.

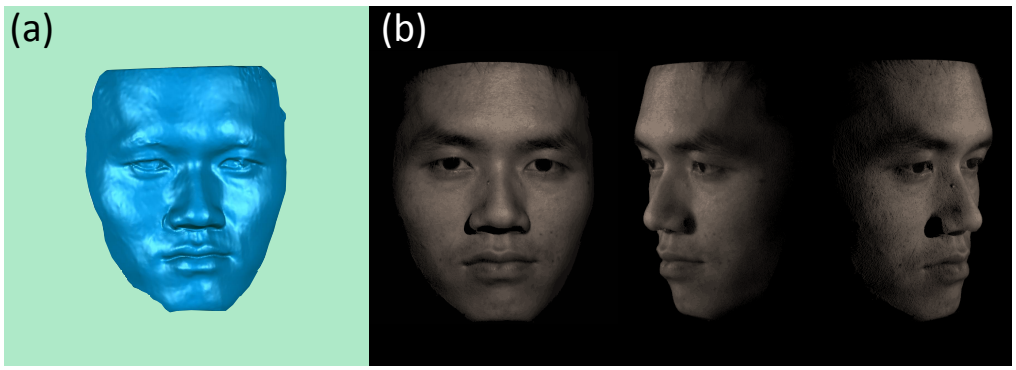

Fig. 9. Human face measurement. (a) Gridding results of human face 3-D point cloud data; (b) Human face 3-D point cloud of different perspectives.

Optics EXPRESS

of its own maximum under different measurement conditions. In this way, the fringe frequency f_{opt} makes the FPP system have a greater robustness. We took such a tedious way to find the f_{opt} was entirely considering rigor. In fact, through a lot of experiments we found that there is an approximate relationship between f_{opt} and the horizontal resolution p_w of projector in experiments: $f_{opt} \approx \frac{p_w}{T}$, where T is fringe period representing the number of pixels per fringe, and its value is usually between 6 and 8. Then, based on the noise models and the principle of TPU, we derived the FFR corresponding to the fringe patterns of different phase-shifting steps, and made simulation to prove the results derived from our theory. The value of the FFR can be used to measure the efficiency of TPU. To unwrap the wrapped phase corresponding to fringe patterns of frequency f_{opt}, we gave priority to 2-step phase-shifting and three-step phase-shifting to generate fringe patterns. The three-step phase-shifting is needed to provide the average intensity for the 2-step phase-shifting. Finally, in order to ensure that there is no temporal noise propagation during the multi-frequency phase unwrapping, we established the relationship between the noise of the low-frequency auxiliary phase and the frequency range of high-frequency fringe patterns whose wrapped phase can be unwrapped correctly by the auxiliary phase. This relationship can be expressed by Eq. (23). We chose to substitute the twice of the detected noise variance of low-frequency absolute auxiliary phase into Eq. (23) to obtain the frequency of high-frequency fringes. There are three reasons for choosing twice of noise variance of the low-frequency absolute auxiliary phase to be the actual noise variance: (1) to improve the system ability to resist noise; (2) twice of the noise variance is sufficient to ensure no temporal noise propagation during the multi-frequency phase unwrapping in most cases; (3) more multiples of the noise variance substituted will lead to more fringe patterns. So that choose twice of noise variance of the low-frequency absolute auxiliary phase to be the actual noise variance is a combination of measurement efficiency and measurement stability.

We proved the results of our theoretical derivation through the relevant experiments. In the quantitative comparison experiment, we compared fringe frequency f_{opt} = 180 periods/frame with frequency 90 periods/frame and frequency 256 periods/frame to prove that using fringe patterns of frequency as coded fringes has the highest measurement precision. There are two points here that need to be highlighted again: (1) f_{opt} = 180 periods/frame is not the only available optimal frequency of fringes that can be used, and it is also possible to refer to other values within the reference range; (2) using the frequency outside the reference range as coded frequency maybe can achieve the same precision as the coded frequency in the reference range under a certain measurement condition, however, for the case of nine kinds of measurement conditions, the frequency in the reference range is the optimal choice.

It is should be noted that we increased the fringe frequency to 180 periods/frame by only 7 frames fringe patterns in our FPP system, and the FPP system achieved the precision ~ 38 μm across a field of view of 400 × 300 × 400 mm. This means that the FPP system can realize high efficiency and high precision 3-D measurements by the scheme we proposed. A human face was measured, and the 3-D reconstruction results demonstrated the success of our proposed scheme, which indicates that our scheme can be applied to practical application such as 3-D face data acquisition. High-precision and effective 3-D data measurement technology can quickly and accurately obtain 3-D geometric data of human face, so as to obtain more effective and accurate 3-D face features. And it will provide a strong support for the subsequent 3-D face recognition, making up the lack of 2-D face recognition by the impact of ambient light and improving the accuracy of face recognition.

Funding

National Key Technologies R&D Program of China (2017YFF0106400, 2017YFF0106403); National Natural Science Fund of China (61505081, 111574152); Final Assembly '13th Five-Year Plan' Advanced Research Project of China (30102070102); Outstanding Youth Foundation of

Optics EXPRESS

Jiangsu Province of China (BK20170034); National Defense Science and Technology Foundation of China (0106173); 'Six Talent Peaks' project of Jiangsu Province, China (2015-DZXX-009); '333 Engineering' Research Project of Jiangsu Province, China (BRA2016407); Fundamental Research Funds for the Central Universities (30917011204, 30916011322); Open Research Fund in 2017 of Jiangsu Key Laboratory of Spectral Imaging & Intelligent Sense (3091601410414).